Luminescence spectroscopy of atomic zinc in rare-gas solids. I

Veronica A. Bracken
Department of Chemistry, National University of Ireland, Maynooth, County Kildare, Ireland

Peter Gürtler
HASYLAB at DESY, Notkestrasse 85, 22603 Hamburg, Germany

John G. McCaffrey[a)]
Department of Chemistry, National University of Ireland, Maynooth, County Kildare, Ireland

(Received 31 March 1997; accepted 1 July 1997)

Steady-state and time-resolved luminescence spectroscopy of atomic zinc isolated in thin film samples of the solid rare gases, prepared by the cocondensation of zinc vapor with argon, krypton, and xenon has been recorded at 6.3 K using synchrotron radiation. Pairs of emission bands result from photoexcitation of the singlet $4p\ ^1P_1 \leftarrow 4s\ ^1S_0$ resonance transition of atomic zinc, even in annealed samples. In Zn/Ar the pair of emission bands were observed in the uv at 218.9 and 238 nm and for Zn/Xe in the near-uv at 356 and 399 nm. For the Zn/Kr system two emission bands were observed in the uv region at 239.5 and 259 nm but in addition, a weaker band was present in the near-uv at 315.6 nm. In a given annealed rare-gas host, the excitation profiles recorded for all the emission bands are identical, exhibiting the threefold splitting characteristic of Jahn-Teller coupling in the triply degenerate excited $^1P_1$ state. These excitation profiles are identified as the solid phase equivalent of the $4p\ ^1P_1 \leftarrow 4s\ ^1S_0$ resonance transition of atomic zinc occurring at 213.9 nm in the gas phase. Based on their spectral positions and temporal decay characteristics, the emission bands observed in the uv and near-uv spectral regions have been assigned as the singlet and triplet transitions, respectively, of atomic zinc. The origin of the pairs of emission bands is ascribed to the Jahn-Teller coupling between noncubic vibronic modes of the lattice and the excited $4p$ orbital of the $^1P_1$ state of atomic zinc, resulting in the coexistence of two energy minima. In Zn/Ar, the effects of slow vibrational relaxation in the excited singlet state were evident in the relative intensities and temporal decay profiles of the pair of emission bands. Specifically, the lower energy emission band was favored with excitation of the highest energy component of the threefold split Jahn-Teller absorption band, while the higher-energy emission was favored with excitation of the lowest-energy component. The intensity of the triplet state emission was observed to be enhanced in the heavier rare gases, being completely absent in Ar, weak in Kr, and the only emission observed in Xe. © *1997 American Institute of Physics.* [S0021-9606(97)00638-7]

I. INTRODUCTION

The first absorption spectra of matrix-isolated atomic zinc were recorded by Duley.[1] In more recent work, absorption and magnetic circular dichroism (MCD) studies of atomic zinc isolated in argon, krypton, and xenon matrices[2] indicated bands, centered at 206.6, 212.3, and 219.8 nm, respectively, exhibiting an increased width relative to the gas phase and a threefold splitting. These absorption bands were assigned as the solid phase equivalent of the $4p\ ^1P_1 \leftarrow 4s\ ^1S_0$ resonance transition of atomic zinc occurring at 213.86 nm in the gas phase.[3] A moment analysis of absorption MCD spectra[2] indicated that Jahn-Teller active, noncubic modes were the source of the threefold splitting. Similar observations have been reported for other excited sp valence systems, such as moment analyses of the MCD spectra of matrix-isolated atomic magnesium, calcium, and strontium in argon examined by Schatz and co-workers.[4] Threefold splitting in matrix excitation spectra have also been recorded in the luminescence studies of the atomic magnesium $3p\ ^1P_1 \leftarrow 3s\ ^1S_0$ transition by McCaffrey and Ozin.[5]

For the Jahn-Teller (JT) modes to be active, the guest atom must be isolated in a symmetrical site of the solid in the ground electronic state with a lowering of symmetry in the excited electronic state arising from coupling to noncubic phonon modes. Definitive assignments of the JT effect have been hampered, however, because of the lack of information about the site of isolation of the guest atom in the solid rare-gas host. The van der Waals radii of metal atoms (M) in the presence of rare-gas (RG) partners are now increasingly available from spectroscopic analysis of the M·RG 1:1 complexes in cold supersonic jets. Such experimental data exist for the diatomic Zn·RG ground $X\ ^1\Sigma_0^+$ state potentials, indicating equilibrium internuclear separations of 4.18, 4.21, and 4.38 Å for Zn·Ar,[6] Zn·Kr,[7] and Zn·Xe,[8] respectively. Since the substitutional site diameters of solid argon, krypton, and xenon are 3.76, 4.01, and 4.35 Å, respectively,[9] the zinc atom is most likely trapped in a single substitutional site in solid rare-gas matrices, being most ''cramped'' in Ar.

Although the absorption spectroscopy of matrix-isolated atomic zinc has previously been published[1,2,10] no luminescence spectroscopy has been reported on this system to date. The luminescence spectroscopy of matrix-isolated atomic

a)Author to whom correspondence should be addressed.

 0021-9606/97/107(14)/5290/10/$10.00

zinc is, in its own right, of fundamental interest in terms of understanding the importance of short- and long-range interactions in solid-state optical spectroscopy. An understanding of solid-state luminescence is facilitated by the previously mentioned large body of accurate data now available on the interaction potentials of diatomic zinc atom/rare-gas atom van der Waals species (Zn·RG). The Zn·RG species have been generated in supersonic expansions by Breckenridge and co-workers[6–8,11,12] and Umemoto *et al.*[13] and the extracted ''pair-potentials'' can be used in well-established[14] theoretical models[15] to simulate the spectroscopy of metal atoms in rare-gas clusters. An extension of this method to the solid state has recently been presented by McCaffrey and Kerins[16] allowing simulation of the luminescence spectroscopy of matrix-isolated atomic zinc.

In the present paper the details of the luminescence spectroscopy of matrix-isolated atomic zinc are examined in steady-state and time-resolved measurements on freshly deposited and annealed samples. A pronounced temperature dependence observed for the pairs of emission bands present in the Zn/RG systems is described in the paper directly following the present and an extension of the theoretical models mentioned in the previous paragraph will be presented[17] in a future publication to explore the origin of these effects.

II. EXPERIMENT

Solid Zn/RG samples were prepared by the cocondensation of zinc vapor, produced by electron bombardment of a 1 mm diameter zinc rod in an Omicron EFM3 UHV evaporator, with the rare gases Ar, Kr, and Xe at 12, 18, and 25 K, respectively. The samples were grown by continuous spray-on of the intersected metal vapor and rare-gas beams onto an LiF window mounted on the cold tip of a Leybold continuous flow UHV liquid helium cryostat, positioned in a UHV vacuum system. An MKS 221A Baratron capacitance manometer, sensitive in the pressure range 0–1000 mbar, was employed to monitor the amounts of rare gas admitted to the gas handling system. A vacuum, monitored with an ionization gauge, on the order of 10^{-8} mbar was achieved prior to cooldown, dropping to 10^{-9} mbar after cooldown. Gas flow rates were controlled by a Granville–Phillips series 203 variable leak valve and were generally in the range of 3.5 to 5 mmol/h for periods of between 10 and 15 min. Rare gases of 99.999% purity were used as supplied by Linde Technische Gase. A 1 mm diameter zinc rod of 99.9985% purity was obtained from Johnson Matthey, Materials Technology, U.K.

Optical measurements were conducted at the HIGITI experimental station in HASYLAB at DESY, Hamburg using synchrotron radiation optimized in the vacuum ultraviolet (vuv) spectral region from the W3 Mini-Wiggler of the DORIS III positron storage ring. The optical layout of the apparatus is shown in Fig. 1. Absorption spectra of matrix-isolated zinc were recorded, by scanning with a 1 m normal incidence modified Wadsworth monochromator. All spectra were scanned linear in wavelength but for the purposes of discussion are presented linear in energy, wave-number

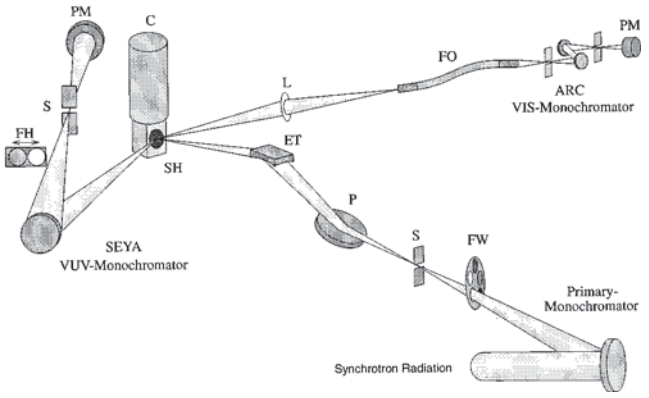

FIG. 1. Schematic of the optical layout of the HIGITI experiment at HASYLAB. The following abbreviations are used in the diagram; FW, filter wheel; S, slit system; ET, focusing mirror; SH, sample holder; C, cryostat; PM, photomultiplier; FH, filter holder; L, lens, and FO, fiber optic.

(cm^{-1}) units. The amount of uv radiation transmitted through the Zn/RG samples was monitored with a Valvo XP2020Q photomultiplier tube detecting the visible emission of a sodium salicylate coating, utilized as a uv photon to visible photon converter, on an exit window.

A reflection technique[18] was used both to monitor sample growth during deposition and evaluate sample thickness after deposition. For absorption spectra, sample thickness was typically 5–8 μm while it was in the 12–16 μm range for luminescence measurements. Utilizing the evaluated sample thickness of the condensed thin films, rough estimates of the number density of atomic zinc in the thin rare-gas films were obtained, from the known gas phase $4p\ ^1P_1 \leftarrow 4s\ ^1S_0$ transition cross section and the recorded absorbance for Zn/RG samples. Typical estimates of the number density of matrix-isolated atomic zinc were in the range 2.4×10^{18}–2.6×10^{18} Zn atoms/cm^3 corresponding to approximate Zn/RG dilution ratios of $1/10^4$.

Steady-state luminescence (emission and excitation) was recorded with either a 0.4 m Seya–Namioka monochromator for the uv region, or a 0.2 m Acton Research Corp. Type VM 502 monochromator for the uv-visible region. A Hamamatsu MCP 1645U-09 microchannel plate and a Hamamatsu R 943-02 photomultiplier tube were used as photon detectors on the Seya–Namioka and ARC monochromators, respectively. Sample annealing was achieved with a heater mounted on the cold tip of the liquid He cryostat and temperatures were measured using a Lakeshore Cryotronics silicon diode.

Lifetime measurements, in the nanosecond range, of the emission observed in the Zn/RG samples were made using the time correlated single photon counting (TCSPC) technique.[19] The synchrotron radiation (SR) generated from the DORIS III storage ring at HASYLAB/DESY is normally operated in the ''5 bunch mode'' with a narrow temporal pulse width (full width at half maximum 130 ps) and a high repetition rate of 5.208 MHz. When run in ''single bunch mode,'' at a reduced repetition rate of 1.042 MHz, lifetimes of up to 10 μs can be measured. A reverse start/stop con-

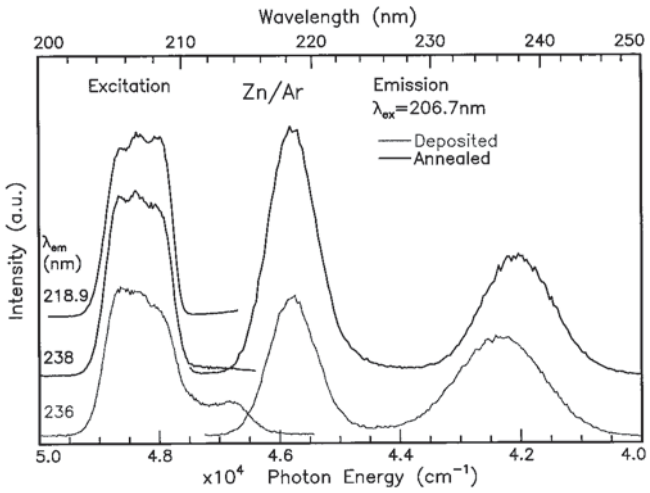

FIG. 2. Emission and excitation spectra recorded at 6.3 K for both thermally stable and unstable sites present in freshly deposited Zn/Ar samples showing the effect of annealing to 33 K for a period of 20 min. The grey traces correspond to the spectra recorded for a freshly deposited sample while the black traces corresponds to the same but annealed sample.

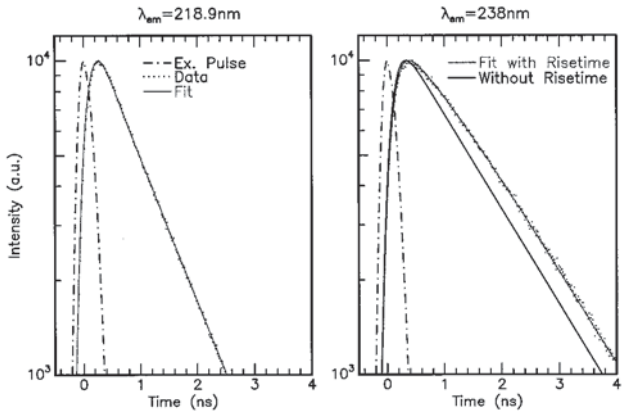

FIG. 3. The decay profiles recorded at 6.2 K of the 218.9 nm and 238 nm emission bands due to 206.7 nm excitation of a Zn/Ar sample annealed to 33 K. Fitting of the entire 218.9 nm decay profile, shown on the left, was achieved using two exponentials where the longer component, with an observed decaytime of 0.93 ns, contributes more than 97% of the emission intensity. The grey trace on the right-hand side corresponds to a double exponential fit of the rise and decay component of the 238 nm decay profile. The black trace is a simulated temporal profile of 238 nm emission generated with the 1.41 ns decay time and convoluted (Ref. 39) with the excitation pulse profile of the synchrotron light source (dot-dash trace), but without a rise time. From a comparison of the fitted (grey) and simulated (black) curves the contribution made by the rise-time component in the 238 nm emission is evident.

figuration of the excitation/emission signals, as described elsewhere,[20] is utilized to reduce ''dead time'' of the time-to-amplitude converter (TAC). Decay times were extracted by fitting trial functions convoluted with the temporal profile of excitation pulse to the recorded decay profiles. The reconvolution and fitting was achieved using the ''ZFIT'' program[21] running on DEC Alpha700 workstations in Maynooth and Hamburg. The fitting criterion was based on an optimization routine minimizing the sum of weighted residuals existing between the fit and the data set. Fits were examined visually from plots of the residuals existing between fits and the recorded decay curves. Acceptable fits were identified when the weighted residuals were randomly distributed about zero. In conjunction with residual plots, the standard ''χ^2 test'' was applied as a numerical guide to aid assessing the quality of the fits. Acceptable χ^2 values lie in the range of 0.8 to 1.2 for deconvoluted decay data exhibiting Poisson statistics.[19]

III. RESULTS

A. Zn/Ar

The emission spectrum recorded at 6.3 K using 206.7 nm photoexcitation of a freshly deposited Zn/Ar sample is shown on the bottom right in Fig. 2. Two emission bands are observed; a narrow band centered at 218.7 nm and a broadband centered at 236 nm. The excitation profile, recorded by monitoring the 236 nm emission band, is shown on the bottom left in Fig. 2. It exhibits hints of threefold splitting centered at 207 nm and a weak sideband centered at 214 nm. When excitation wavelengths of 212 and 214 nm were selected,[22] broad, weak emission bands centered at 232 and 234 nm were observed.

The changes produced in the emission spectra as a result of annealing a freshly deposited Zn/Ar sample to 33 K for approximately 20 min are shown by the black trace on the right in Fig. 2 where a narrowing and a redshift from 236 to 238 nm is observed in the lower energy band after annealing. The uv emissions of the annealed Zn/Ar sample exhibit an increase in absolute intensity relative to the emissions of the freshly deposited sample. The narrowing and shifting of the lower energy uv emission band to the 238 nm band occurring upon sample annealing is attributed to the removal of the thermally unstable sites emitting at 232 and 234 nm.

Annealing had a more pronounced effect on the excitation spectra whereby the broad feature centered at 214 nm in the excitation profile, recorded by monitoring 236 nm emission, vanished as shown by the middle black trace on the left in Fig. 2. The band centered at 206.7 nm, now clearly exhibiting a threefold splitting, is the only band observed to remain after annealing. Excitation into the central component of the threefold splitting at 206.7 nm produced the pair of uv emission bands at 218.9 and 238 nm as depicted by the upper black trace on the right in Fig. 2. The excitation profiles recorded for the 218.9/238 nm pair of emission bands exhibited threefold splitting at identical wavelength values, i.e., 205.5, 206.7, and 208.2 nm but, conspicuously, the relative intensities of the blue and red features in the threefold split profiles differed, as shown on the top left in Fig. 2. A summary of all the positions in the threefold split excitation profiles are listed in the left hand column of Table I.

A portion of the temporal decay curve recorded at 9 K for the 218.9 nm emission as a result of 206.7 nm excitation is shown on the left in Fig. 3. The decay time was found to be 0.93 ± 0.09 ns using a double exponential fit over the entire decay profile recorded. This value was found not to vary for samples prepared under the same conditions and compo-

TABLE I. A summary of the wavelength positions of maximum intensity of the threefold split excitation profiles in the Zn/RG systems. The corresponding rise and decay times identified in the emission bands with narrow-band excitation of the listed absorption features are also listed. For the low-energy emission bands the contributions the rise and decay components make to the temporal profiles are given in the column on the right as the ratios of the amplitudes of the fitting functions.

		High energy		Low-energy emission			
Zn/RG	λ_{ex} (nm)	λ_{em} (nm)	τ (ns)	λ_{em} (nm)	τ_R (ns)	τ_D (ns)	A_R/A_D
Zn/Ar	205.5	218.9	0.935	238.0	0.62	1.41	−0.313
	206.7		0.935		0.63	1.41	−0.328
	208.2		0.935		0.66	1.41	−0.360
Zn/Kr	211.5	239.5	1.265	259.0	1.49	1.60	−0.589
	212.4		1.265		1.49	1.60	−0.579
	213.5		1.265		1.49	1.60	−0.564
Zn/Xe	219.1	356.0	$>10\ \mu$s	399.0		$>10\ \mu$s	
	219.9		$>10\ \mu$s			$>10\ \mu$s	
	220.7		$>10\ \mu$s			$>10\ \mu$s	

sition and contributed to over 97% of the decay profile as indicated in Table I. However, in the case of the 238 nm emission a component corresponding to a rise time of 0.63 $\pm$0.06 ns was identified in the decay profile recorded at 9 K in conjunction with a decay time of 1.41$\pm$0.1 ns. The contribution this rise-time component makes in the 238 nm decay profile is clearly illustrated by the ''bulge'' evident in the observed data shown on the right in Fig. 3 when compared to a decay profile simulated with a single decay time of 1.41 ns.

B. Zn/Kr

Photoexcitation at 212.4 nm, a wavelength value identified in the absorption spectrum of Zn/Kr on deposition, produced the emission spectrum shown by the bottom trace on the right of Fig. 4. The spectrum comprises of a pair of emission bands in the uv at 259 and 239 nm and two weaker emission features in the near-uv region at 315 and 344 nm. The excitation spectrum recorded for the 259 nm emission band is shown on an expanded energy scale on the bottom in Fig. 4. A more resolved excitation profile exhibiting a threefold splitting centered at 212.4 nm was recorded by monitoring the 315 nm emission band. Considerably broader excitation profiles extending to the red of the main feature centered at 212.4 nm were recorded[22] by monitoring the weaker emission bands at 239 and 344 nm. The emission spectrum produced with excitation in the redwing of the excitation profile at 218 nm contained two emission features centered at 252 and 344 nm.

The comparison, shown on the right in Fig. 4, of the emission spectra recorded with photoexcitation at 212.4 nm on deposition and after warming to 45 K demonstrates the effect of annealing on Zn/Kr samples. A more resolved pair of uv emission bands and only a single near-uv emission band remains after annealing, as indicated by the black trace shown on the right in Fig. 4. Due to the absence of the uv emission band at 252 nm and the weak near-uv emission band at 344 nm, a significant increase was observed in the total intensity of the emission bands remaining after annealing. It is concluded then that the former emission bands are associated with the occupancy of atomic zinc in thermally unstable sites present in the freshly deposited Zn/Kr sample. The most pronounced change in the excitation spectra shown on the left of Fig. 4 is evidenced by the absence of the composite feature absorbing at 218 nm when the 259 nm emission was monitored before and after annealing. The positions of the resolved threefold splittings exhibited by each excitation spectrum in the annealed Zn/Kr samples are identical as shown on the left in Fig. 4, having values of 211.5, 212.4, and 213.5 nm as given in Table I.

Decay times of the 239.5 and 259 nm emission bands were found after fitting the recorded decay profiles with

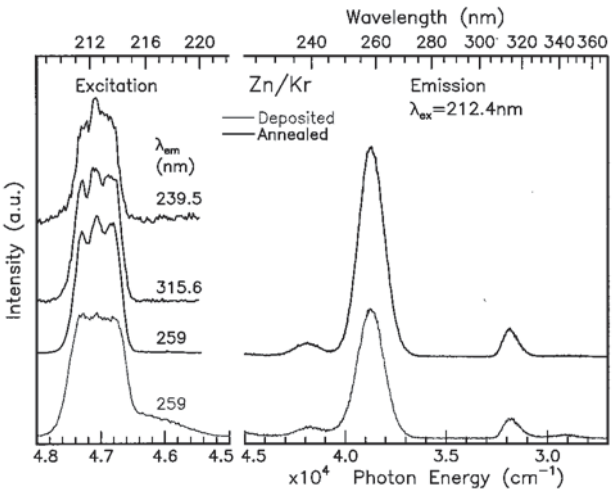

FIG. 4. Steady-state luminescence spectra recorded at 6.3 K for a freshly deposited Zn/Kr sample. A comparison of the emission recorded before and after annealing due to excitation at 212.4 nm is shown on the left. The grey trace corresponds to a freshly deposited Zn/Kr sample while the black trace was recorded under the same conditions after annealing to 45 K for a 20 min period. The corresponding simplified excitation spectra are shown on the left.

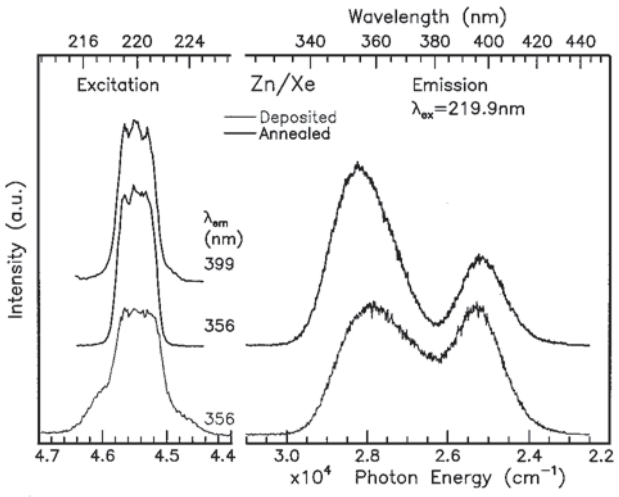

FIG. 5. The effect of sample annealing on the excitation and emission spectra of Zn/Xe. The grey traces corresponds to a freshly deposited Zn/Xe while the black traces were recorded after the sample was annealed to 65 K for 20 min and scanned at 9 K. The absence of the wings in the excitation profiles of annealed Zn/Xe and the emission spectra exhibiting a more resolved splitting are attributed to the removal of thermally unstable sites emitting at 380 nm.

double exponential functions. The decay time of the 239.5 nm emission band was taken as 1.265 ns as this component contributed over 97% of the intensity. The decay of the 259 nm band comprised of a rise time of 1.49 ns and a decay time of 1.60 ns as listed in Table I. Decay time measurements of the near-UV emissions at 315 nm could not be made using the TCSPC technique as the decay times were longer than the time between the excitation pulses, even with the storage ring operating in the ''single-bunch'' mode. With a repetition rate of 1.042 MHz in single bunch mode, it is estimated that the decay time of the 315 nm emission is longer than 10 μs.

C. Zn/Xe

Shown on the bottom right in Fig. 5, is the emission spectrum recorded for atomic zinc isolated in a freshly deposited xenon matrix. Two emission features of approximately equal intensity but different linewidths are observed in the near-UV at 356 and 395 nm with excitation at 219.9 nm. In contrast to the Zn/Ar and Zn/Kr systems, no emission was detectable in the uv region for Zn/Xe. The excitation profile recorded for the 395 nm emission band was similar to that shown in the bottom trace of Fig. 5 for the 395 nm band exhibiting broad wings on the low- and high-energy side of the main feature centered at 220 nm. Emission spectra recorded with photoexcitation of these wing features at 216.2 and 224 nm contained[22] single, broad emission bands slightly shifted ($500\ \mathrm{cm}^{-1}$) relative to one another at 380 nm. Red wing excitation produced the lower-energy emission band, blue wing excitation favored the higher-energy band.

Annealing freshly deposited Zn/Xe samples to 65 K produced significant changes in the emission spectra. A comparison of the emission spectrum recorded at 9 K after annealing with that recorded on deposition with the same 219.9 nm excitation, shown on the right in Fig. 5, reveals the following changes. The splitting of the emission bands is more pronounced in the annealed sample, the intensity of the 356 nm emission band increases and the wavelength of maximum intensity of the lower-energy band shifts from 395 to 399 nm. The effect of annealing on the excitation spectra was manifested by the absence of the wings on the high- and low-energy sides of the excitation profile as illustrated by comparing the middle and lower traces in Fig. 5. From these observations it can be inferred that thermally unstable sites are responsible for the 380 nm emission bands in freshly deposited Zn/Xe samples. The presence of these emission bands results in a less pronounced splitting between the 356 and 399 nm bands in the emission spectra of freshly deposited samples and arises from absorption of the broad feature responsible for the wings of the excitation spectra. Identical excitation spectra were recorded for the pair of emission features at 356 and 399 nm in annealed Zn/Xe as shown on the left of Fig. 5. The positions of the features in the threefold split excitation profile in annealed Zn/Xe are 219.1, 219.9, and 220.7 nm as quoted in Table I. Because of the identical form of the excitation spectra recorded for the pair of emission bands, it is inferred that a single optical center is responsible for the 356 and 399 nm pair of emission bands in annealed Zn/Xe. Decay times of the near-UV emission bands could not be measured using the TCSPC technique for the reason mentioned earlier for the near-UV emission bands in Zn/Kr.

IV. DISCUSSION

A. Spectral assignments

A summary of the excitation and emission spectra recorded in annealed Zn/RG samples is presented in Fig. 6 as well as the positions of the gas phase singlet and triplet resonance transitions of atomic zinc. The excitation bands, centered at 206.7, 212.4, and 219.9 nm in argon, krypton, and xenon, respectively, are, in accordance with previous absorption studies, identified as the solid phase equivalent of the $4p\ ^1P_1 \leftarrow 4s\ ^1S_0$ resonance transition of atomic zinc occurring at 213.86 nm in the gas phase.[3] The characteristic threefold splitting evident in the excitation profiles of the $^1P_1 \leftarrow {}^1S_0$ transition of matrix-isolated atomic zinc has been attributed to the dynamic Jahn-Teller effect[2] in previous MCD studies. As shown in Fig. 6, the excitation band of atomic zinc in solid argon exhibits a blueshift relative to the gas phase $^1P_1 \leftarrow {}^1S_0$ transition, while in xenon, an equivalent redshift is observed. In krypton matrices, the resonance transition is only slightly blueshifted from the gas phase absorption as indicated in Fig. 6. Data obtained from spectroscopic studies of the diatomic Zn·RG van der Waals complexes allow an interpretation of this behavior.

The equilibrium internuclear separations in the ground $X\ ^1\Sigma_0^+$ states of the Zn·RG diatomics are 4.18, 4.21, and 4.38 Å in Zn·Ar,[6] Zn·Kr,[7] and Zn·Xe,[8] respectively, while the substitutional site diameters of argon, krypton, and xenon are 3.76, 4.01, and 4.35 Å at 4 K.[9] A comparison of the equilib-

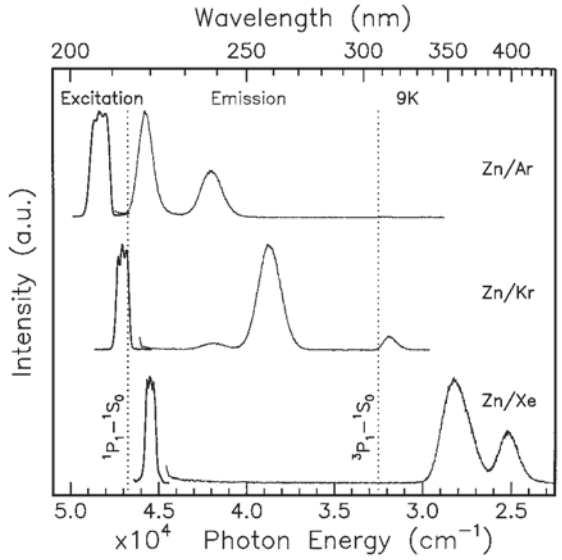

FIG. 6. A summary of the excitation and emission spectra recorded at 9 K in annealed Zn/RG samples. The excitation spectra are shown in black on the left of the figure while their corresponding emission spectra are shown on the right in grey. The gas phase singlet $4p\ ^1P_1$-$4s\ ^1S_0$ and triplet $4p\ ^3P_1$-$4s\ ^1S_0$ resonance transitions of atomic Zn are indicated by the vertical dotted lines for comparison.

rium internuclear separation of diatomic Zn·Ar to the substitutional site diameter of solid argon indicates that atomic zinc will be isolated ''cramped'' in a single substitutional site of argon. The extent of crampness is much less in Kr and an almost perfect size match exists in the case of Zn/Xe. The degree of cramped isolation of atomic zinc in the solid is reflected in the extent of blueshifting of the matrix excitation profiles relative to the gas phase absorption, suggesting that atomic zinc is trapped in single substitutional sites for all the rare-gas solids Ar, Kr, and Xe.

Using experimentally determined pair potentials for the bound $X\ ^1\Sigma_0^+$ and $C\ ^1\Pi_1$ states of the Zn·RG diatomics and high-level *ab initio* calculations for the repulsive $D\ ^1\Sigma_0^+$ states, McCaffrey and Kerins[16] have calculated the absorption energies of the Zn/RG matrix systems to be 203.3, 204.1, and 215.7 nm for Ar, Kr, and Xe hosts, respectively. These values are all slightly to the blue of the observed transitions but they do support the simple ideas concerning the increased importance of long-range attraction over short-range repulsion which is expected to dominate in the larger sites of the heavier rare-gas solids.

Excitation into the central component of the threefold splitting of atomic zinc isolated in argon, krypton, and xenon produced the emission spectra shown by the grey traces on the right in Fig. 6. The decay times extracted from time-resolved measurements of the uv emissions in Zn/Ar (218.9/238 nm) and Zn/Kr (229.5/259 nm) are collected in Table II. The values listed in Table II were recorded in annealed samples and found not to vary at the low (6–10 K) temperatures at which the present measurements[23] were made. The decay times recorded for the emission bands are thereby taken as the radiative lifetime of the $4p\ ^1P_1$ excited

TABLE II. Photophysical characteristics of the luminescence bands of the atomic zinc matrix isolated in argon and krypton at 6.3 K and in xenon at 9 K.

Zn/RG	λ_{ex} (nm)	λ_{em} (nm)	τ (ns)	Bandwidth (cm^{-1})	Stokes' shift (cm^{-1})
Gas phase	213.86	213.86	1.41		
		307.59	30.4 μs		
Zn/Ar	206.7	218.9	0.93	1154	2696
		238.0	1.41, 0.63[a]	1642	6362
Zn/Kr	212.4	239.5	1.26	1555	5327
		259.0	1.60, 1.49[a]	1501	8471
		315.6	>10 μs	1243	825[b]
Zn/Xe	219.9	356	>10 μs	1724	4421[b]
		399	>10 μs	1395	7448[b]

[a]Corresponds to the magnitude of the rise-time component.
[b]Estimates relative to the gas phase $4p\ ^3P_1 \leftarrow 4s\ ^1S_0$ absorption of atomic zinc at 307.59 nm.

state of Zn in the matrix. In Fig. 7, these matrix lifetimes τ_{obs} are shown compared with the emission wavelength dependence (a λ^3 extrapolation[24]) of the $4p\ ^1P_1$ excited state lifetime of atomic zinc having a gas phase value of 1.41 ns at 213.86 nm. It is clear in Fig. 7 that the observed matrix lifetimes, shown by the squares, are significantly less than the λ^3 extrapolation curve of the gas phase lifetime, indicated by the open diamond.

When the matrix emission lifetimes are corrected for the effective field of the Ar and Kr hosts, the values indicated in Fig. 7 by the filled circles result. Correction of the observed matrix lifetimes τ_{obs} is made[25,26] with the formula

$$\tau_{cor} = \tau_{obs} n[s(n^2-1)+1]^2, \tag{1}$$

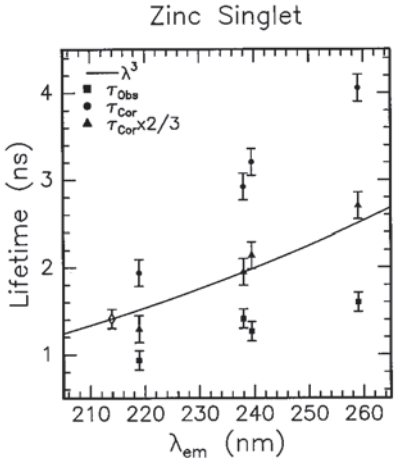

FIG. 7. A comparison of the λ^3 dependence of the radiative lifetime of the $4p\ ^1P_1$ state of atomic zinc in the gas phase and the lifetimes recorded for the pairs of emission bands in the Zn/Ar and Zn/Kr systems. The raw matrix data is shown by the squares, the data corrected for the effective field of solid is shown by the circles. The effective field correction is implemented using the index of refraction n of the solid with Eq. (2) given in the text. Reduction of the corrected lifetime by 2/3 yields the best agreement between the matrix lifetimes and the λ^3 extrapolation of the gas phase lifetime.

which involves the use of the indices of refraction[27] of the rare-gas hosts, n at the wavelengths where the emissions are observed and at the temperature of the measurements (6.3 K). The s parameter is a depolarization factor related to the symmetry of the site accommodating the optically active guest atomic zinc. If the depolarization factor is isotropic, as it is in a substitutional site of the rare-gas lattice, s has a value of 1/3. On the basis of the comparison made earlier of the diatomic Zn·RG van der Waals bond lengths and the substitutional site diameters of the solid rare gas, use of an s value of 1/3 results in a correction formula of the form

$$\tau_{\mathrm{cor}} = \tau_{\mathrm{obs}} n[(n^2+2)/3]^2. \tag{2}$$

Comparison of the effective field corrected matrix lifetimes τ_{cor}, shown as filled circles in Fig. 7, and the λ^3 curve would indicate that the lifetime of the $4p\ ^1P_1$ excited state of atomic zinc is longer in the solid than in the gas phase. Use of s values of 0 gives reasonable agreement between the corrected lifetimes and the λ^3 plot. However, $s=0$ values pertain to physical systems which have depolarization in two dimensions only and which is not appropriate to the Zn/RG systems. Values other than 1/3 (1/2 or 1), associated with reduced dimensionality make the comparisons between the matrix lifetimes and gas phase value even worse. As it is highly unlikely that the overlap between the $4p$ and $4s$ orbitals on atomic zinc is reduced in the solid rare gases, some other interaction must be producing the observed difference in the Einstein A coefficient of the $4p\ ^1P_1 \rightarrow 4s\ ^1S_0$ resonance transition of atomic zinc in the gas phase and solid matrices. If the corrected matrix lifetimes are multiplied by 2/3 all the matrix data fall on the λ^3 extrapolation curve as shown by the triangles in Fig. 7. The origin of this factor is presently unclear, however, the overall agreement of the matrix and gas phase lifetimes indicates that the pair of uv emission bands in Zn/Ar and Zn/Kr correspond to the $4p\ ^1P_1 \rightarrow 4s\ ^1S_0$ fluorescence transition of atomic zinc.

Time-resolved measurements of the near-uv emissions could not be recorded as the repetition rate of the storage ring was too high, even operating in ''single-bunch'' mode at a frequency of 1.042 MHz. This behavior and their spectral locations strongly suggest that the near-uv emission bands present in Zn/Kr and Zn/Xe correspond to the triplet $4p\ ^3P_1 \rightarrow 4s\ ^1S_0$ phosphorescence transition of atomic zinc occurring at 307.6 nm in the gas phase[3] and having a radiative lifetime[28] of 30.4 μs.

B. Origin of pairs of emission bands

The existence of pairs of bands in the luminescence of the Zn/RG systems, both of which are assigned to the same electronic transition, is, to the authors' knowledge, unique in the matrix spectroscopy of metal atoms isolated in a single site of the solid rare gases. Spectral assignments of the uv emission pair in Zn/Ar and Zn/Kr to the $4p\ ^1P_1 \rightarrow 4s\ ^1S_0$ transition and the near-uv emission band pair in Zn/Xe to the $4p\ ^3P_1 \rightarrow 4s\ ^1S_0$ transition of atomic zinc have been made above but the origin of the duplication of the gas phase transition in the solid has not yet been established. Based on the fact that these matrix emission pairs are produced by excitation of absorption bands for which excited state Jahn-Teller coupling has been identified, it would seem plausible to propose that they arise from the existence of two energetically distinct Jahn-Teller minima on the excited $4p\ ^1P_1$ state surface of atomic zinc in the solid rare-gas matrix.

A similar phenomenon, i.e., pairs of emission bands assigned to the same electronic transition, has been observed in the luminescence spectroscopy[29] of alkali halide solids doped with the heavy metal ions Tl^+, In^+, Ga^+, Sn^{2+}, and Pb^{2+}. All of these systems have, like neutral atomic zinc, an s^2 lowest-energy electronic configuration, but in particular, the work done on Ga^+, which is isoelectronic with atomic Zn, is suitable for comparison with the Zn/RG luminescence. In the KBr:Ga^+ system a pair of emission bands designated as A_T (high energy) and A_X (low energy), are produced both directly via $A\ (^3T_{1u} \leftarrow {}^1A_{1g})$ excitation and indirectly with $C\ (^1T_{1u} \leftarrow {}^1A_{1g})$ band excitation.[30] Polarization,[31] MCD[32] measurements, and optical detection of the excited state magnetic resonance[33] of single crystals of these solids provided a wide range of experimental evidence for the existence of the pairs of emission bands and in conjunction with theory, allowed identification of their origin. The origin of the pair of A emissions was presented in the theoretical work of Fukuda[29] and Ranfagni *et al.*[34] as the existence of two minima on the $^3T_{1u}$ state adiabatic potential energy surface (APES). The minima were identified as having tetragonally and trigonally distorted geometries around the optically active center due to the strong Jahn-Teller coupling of the electronic triplet state of the guest metal ion and the ϵ_{2g} and τ_{2g} vibronic modes of the alkali halide lattice.

Another feature of the Ga^+, In^+, and Tl^+ metal ions in KI, KBr, KCl, and NaCl (Ref. 35) phosphor systems characteristic of the dynamic Jahn-Teller effect, is the observation of symmetric threefold splitting on the C state $(^1T_{1u} \leftarrow {}^1A_{1g})$ absorption bands. Similarly, all the corresponding spin singlet $(^1P_1 \leftarrow {}^1S_0)$ excitation spectra recorded for the luminescence in the Zn/RG systems exhibited this symmetric threefold splitting.

In the Zn/RG luminescence, the Zn/Xe system exhibits a pair of phosphorescence bands, or A band emissions in the terminology of alkali halide systems doped with heavy metal ions. Based on the above criteria, it is expected that at least in the Zn/Xe system Jahn-Teller coupling results in two geometrically distinct minima on the $^3T_{1u}$ APES, since the spin–orbit[36] coupling constant of atomic zinc is small $(386\ \mathrm{cm}^{-1})$ with respect to its exchange interaction $(7024\ \mathrm{cm}^{-1})$. Similarly, the observation of two uv emission bands assigned to singlet $^1P_1 \rightarrow {}^1S_0$ transition in the Zn/Ar and Zn/Kr systems suggests the coexistence of two nondegenerate minima also on the $^1T_{1u}$ APES.

C. Similar excitation spectra for Jahn-Teller emission bands

Comparison of the excitation spectra recorded for the 219/238 nm pair of emission bands in annealed Zn/Ar, shown in Fig. 2, indicates that the wavelength positions of

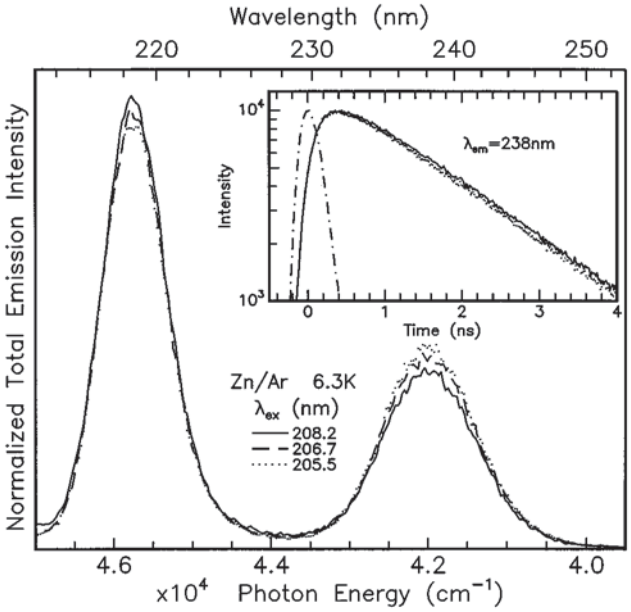

FIG. 8. Emission spectra recorded for an annealed Zn/Ar sample at 6.3 K following excitation of the Jahn-Teller components. The spectra are shown having normalized total emission intensities for the purpose of comparison. Shown in the inset are the corresponding decay profiles of the 238 nm emission band.

maximum intensity of the threefold splittings are identical but the relative intensities of the three components varied depending on which emission band was monitored. Thus when the 218.9 nm emission band was monitored the lowest-energy excitation component at 208.2 nm was observed to dominate and when the 238 nm emission was monitored, the highest-energy component at 205.5 nm dominated. A detailed comparison of the emission resulting from narrow-band (0.2 nm) excitation into each of the three splittings of Zn/Ar is shown for normalized total emission intensities in Fig. 8. The 218.9 nm emission band is favored with excitation of the lowest-energy component at 208.2 nm (solid line) while the intensity of the 238 nm emission is observed to increase when 205.5 nm excitation (dotted line) is used. Emission bands of intermediate intensity result with excitation of the central feature at 206.7, as shown by the dashed line in Fig. 8. In contrast to the Zn/Ar system, excitation into the three Jahn-Teller components of the Zn/Kr and Zn/Xe excitation profiles resulted in identical emission spectra.

In both the Zn/Ar and Zn/Kr singlet emission systems, rise times were identified in the decay curves of the low-energy emission band. Identical rise-time components of 1.49 ns were identified in the decay curves of the 259 nm emission in Zn/Kr, with photoexcitation into each of the Jahn-Teller splittings. Slight differences exist in the shapes of the decay profiles of the 238 nm band in Zn/Ar as a result of excitation of the three absorption components, as shown in the inset of Fig. 8, but the extracted rise times are, as quoted in Table I, the same within the present experimental error. The differences in the shapes of the decay profiles arise from varying contributions of the 0.6 ns rise-time component with excitation of the Jahn-Teller components. The ratio of the amplitudes of the rise and decay components in the 238 nm band are shown in the column on the right-hand side of Table I. The contribution of the slow rise component in the 238 nm emission band is largest with 208 nm excitation, and smallest with 205.5 nm excitation, behavior consistent with that exhibited in the intensity measurements.

In contrast to the low-energy emission bands, no rise times were detected for the decay of the high-energy emission bands in either the Zn/Ar or Zn/Kr systems. Moreover, since the low-energy 259 nm emission dominated in Zn/Kr, with its slow rise time of 1.49 ns, unlike its 238 nm counterpart in Zn/Ar, which was weaker yet showing a fast rise time of 0.6 ns, it is inferred that the relative intensity of the pair of emission bands in both the Zn/Ar and Zn/Kr systems is not dependent on the magnitude of their rise times. Rather, the relative intensities would appear to be controlled by the branching ratio of the relaxation routes occurring immediately after optical excitation on the excited surface.

Supporting evidence for this suggestion is provided in a comparison of the relative rise times extracted from fits of the decay curves of the 238 nm emission of Zn/Ar to the relative intensities of the 238 nm emission band produced with photoexcitation into the Jahn-Teller components. Explicitly, excitation into the highest energy Jahn-Teller component produced the most intense 238 nm emission band but exhibited a similar rise time, confirming that the intensity of the emission bands are not controlled by the rise times. The contributions of the rise times in the decay profiles for specific excitation of the Jahn-Teller absorptions of Zn/Ar and Zn/Kr are presented in Table I.

The simplest kinetic model which could describe the temporal characteristics of two emission bands originating from a single excitation and terminating on the same ground state is a four level, four step scheme. The time dependence of the population in these levels are obtained by the mathematical expressions pertaining to the integrated rate expressions of the four levels involved, and are given in the Appendix of the following paper.[23] Inspection of the expressions for the time dependence of the two emitting levels indicates that the rise times in both of these levels must be identical if single steps leading to their formation after excitation exist in competition. Clearly this is not the case in either Zn/Ar and Zn/Kr as the higher-energy emission bands do not exhibit rise times, on the 100 ps resolution of the present measurements, while the lower energy bands do. Consequently an additional rate determining step must be introduced in the relaxation process populating the lower-energy emitting levels in both the Zn/Ar and Zn/Kr systems.

D. Photophysical characteristics

A summary of the bandwidths and Stokes' shifts observed at 6.3 K for atomic zinc luminescence in annealed samples of the solid rare gases Ar, Kr, and Xe are given in Table II. For the Zn/Ar system, a bandwidth (full width at half maximum) of 1154 cm^{-1} was measured for the emission band centered at 218.9 nm while the emission band centered at 238 nm had a larger bandwidth of 1642 cm^{-1}. The Stokes'

shift of the 218.9 and 238 nm emission bands were found to be 2696 and 6362 cm^{-1}, respectively, relative to the central component in the matrix singlet absorption at 206.7 nm.

In the Zn/Kr system, a bandwidth of 1555 cm^{-1} was measured for the emission band centered at 239.5 nm, which is slightly larger than the value of 1501 cm^{-1} recorded for the 259 nm band. The Stokes' shifts for the 239.5 and 259 nm emissions were found to be 5327 and 8471 cm^{-1}, respectively, relative to excitation at 212.4 nm. The triplet emission band of Zn/Kr at 315.6 nm had a narrower bandwidth of 1243 cm^{-1} than either of the pair of singlet emissions. The intrinsic Stokes shift of the 315.6 nm triplet emission band could not be determined since the triplet transition has not been observed in either absorption or excitation spectra. However, as an estimate of its magnitude, a Stokes shift of 825 cm^{-1} is obtained relative to the gas phase $4p\ ^3P_1 \leftarrow 4s\ ^1S_0$ triplet absorption at 307.59 nm, again considerably smaller than the Stokes shift of the singlet bands.

The widths of the emission bands of Zn/Xe centered at 356 and 399 nm bands were 1724 and 1395 cm^{-1}, respectively. Since direct triplet absorption was not observed, estimates of the Stokes shift of 4421 and 7448 cm^{-1} for the 356 and 399 nm emission bands, respectively, are evaluated relative to the gas phase triplet absorption.

The differences in the bandwidth exhibited by the Zn/RG emission system will now be examined qualitatively within the framework of a configurational coordinate model and the Franck–Condon principle. In this model transitions are assumed to originate from the lowest phonon level, since the temperature of the system (6 K) is approaching absolute zero. The width of an emission band is governed then by the spatial extent of the excited state $v=0$ vibrational wave function and the degree of curvature of the ground-state potential energy surface accessed by the vertical transition. Thus the 238 nm emission of the Zn/Ar system, with its larger bandwidth, couples to a more strongly repulsive region of the ground-state potential energy surface than the narrower 218.9 nm band. As shown schematically in Fig. 9, the luminescence characteristics of the Zn/Ar system can therefore be accommodated in a single configuration coordinate (SCC) model.

The emission characteristics in the Zn/Kr singlet system cannot be described in a SCC model as the higher-energy 239.5 nm band exhibits a slightly larger bandwidth than the lower energy 259 nm band. The triplet emissions of Zn/Xe behave in a more extreme fashion in that the higher-energy emission has, as listed in Table II, a much larger bandwidth than the lower-energy emission band. Thus one is forced to conclude that a *single* configurational coordinate model does not even qualitatively describe the photophysical characteristics of the Zn/RG emissions.

The larger Stokes' shifts and bandwidths observed for the singlet emissions rather than the triplet emission in the Zn/Kr system indicate a larger difference in the strength of the electron–phonon coupling in the two electronic levels coupled in the singlet transition rather than in the triplet transition. This difference can be correlated with the different extents of the $4p$ wave function in the two spin states, i.e.,

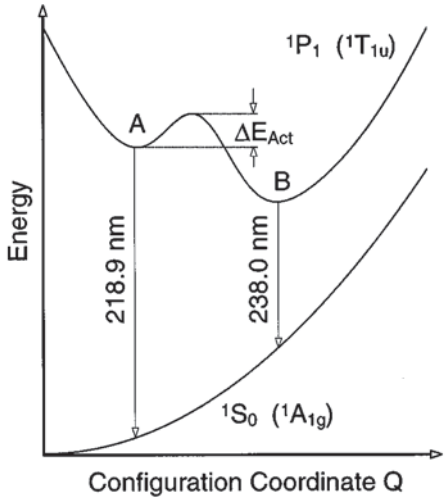

FIG. 9. A schematic configurational coordinate diagram for the pair of Jahn-Teller minima of the Zn/Ar system existing on the $^1T_{1u}$ APES and yielding the 218.9 and 238 nm emission bands. The intervening barrier between the two emitting levels is indicated by ΔE_{Act}, the magnitude of which is determined in the temperature-dependent measurements presented in the paper directly following.

the larger radial extent[37] of the $4p$ orbital in the $^1P_1$ state than in the $^3P_1$ state. Hence the former would be expected to have a stronger interaction with its surroundings than the latter, since, for example, in the diatomic Zn·Kr (Ref. 7) system, the singlet $4s4p\ ^1\Pi_1$ molecular state has a binding energy of 1400 cm^{-1}, while that of triplet $4s4p\ ^3\Pi_1$ state is only 800 cm^{-1}.

V. CONCLUSIONS

Excitation spectra recorded for the luminescence observed for atomic zinc isolated in each of the cryogenic matrices Ar, Kr, and Xe show a threefold splitting due to the dynamical Jahn-Teller effect. These excitation bands are identified as the matrix equivalent of the gas phase $4p\ ^1P_1 \leftarrow 4s\ ^1S_0$ resonance transition of atomic zinc. From a combination of steady-state and time-resolved luminescence spectroscopy, the uv and near-uv emissions are assigned to the singlet and triplet transitions for atomic zinc in the solid rare gases. With these spectral assignments, the pairs of emission bands present in the solid rare gases correspond to a single gas phase electronic transition of atomic zinc.

Based on the similarity of the Zn/RG luminescence with the isoelectronic species Ga^+ in alkali halides, the origin of the pairs of the emission bands in the Zn/RG systems is attributed to the dynamic Jahn-Teller coupling between the excited $^1P_1$ state of atomic zinc and the vibronic modes of the RG solid resulting in the coexistence of two minima of different symmetry and energy on the $^1T_{1u}$ APES. Theoretical analysis[16] of the luminescence in the Zn/RG systems, based on the use of accurate Zn·RG pair potentials, indicates that the presence of the pair of uv and the pair of near-uv emission bands arises from very strong Jahn-Teller stabilization on the excited $^1T_{1u}$ and $^3T_{1u}$ state, respectively, leading to the coexistence of distinct energy minima.

Rise-time components evident in the temporal decay profiles of the low-energy uv emission bands in the Zn/Ar and Zn/Kr systems indicate that the rate of vibrational relaxation on the excited state surface occurs on a nanosecond time scale. No rise-time effects were observed for the higher-energy emission bands suggesting that vibrational relaxation occurs for this level time scale at less than 100 ps. From the gradients calculated[17] for the potential energy surfaces leading to the Jahn-Teller stabilized minima, the presence of a rise time in the low-energy emission bands of the Zn/RG systems is accounted for, as well as its absence in the high-energy emission band.

The differences in the efficiency of spin singlet to triplet intersystem crossing exhibited in the luminescence of the Zn/RG systems correlates with pump–probe studies on the diatomic Zn·RG van der Waals species[6,8,7,12] whereby spin–orbit predissociation of the bound $^1\Pi_1$ state occurring from a crossing with the repulsive $^3\Sigma_1$ state results in the production of atomic zinc $^3P_{1,2}$ states. More recently, theoretical models for atomic zinc isolated in the rare-gas solids,[16] based on the use of Zn·RG pair potential data[38] in $Zn(RG)_n$ clusters, were used to investigate the dynamical effects observed in the solid-state Zn/RG luminescence. Preliminary results indicate that the external heavy atom effect is not responsible for the enhancement of the ISC in the heavier rare-gas hosts, rather it is determined by the presence of spin singlet/spin triplet surface crossings at lower energies in the heavier hosts than in the lighter rare gases.

ACKNOWLEDGMENTS

We would like to acknowledge Dr. S. Moeller for his technical assistance during the course of this work and for supplying us with Fig. 1. This research was funded by the EU HC&M 1993-'95 ''Access to Large Scale Facilities'' Programme. V.B. and P.K. gratefully acknowledge receipt of Irish Government Forbairt Basic Science studentships.

[1] W. W. Duley, Proc. Phys. Soc. **91**, 976 (1967); Nature **210**, 264 (1966).
[2] B. Hoffmann-Millack, A. Klein, H. Lagier, B. Maid, and J. Hormes, Chem. Phys. **136**, 453 (1989).
[3] C. E. Moore, *Atomic Energy Levels*, National Bureau of Standards Circular Number 467 (U.S. Government Printing Office, Washington D.C., 1957), Vol. 1, p. 125.
[4] J. C. Miller, R. L. Mowery, E. R. Krausz, S. M. Jacobs, H. W. Kim, P. N. Schatz, and L. Andrews, J. Chem. Phys. **74**, 6349 (1981).
[5] J. G. McCaffrey and G. A. Ozin, J. Chem. Phys. **101**, 10354 (1994).
[6] I. Wallace, R. R. Bennett, and W. H. Breckenridge, Chem. Phys. Lett. **153**, 127 (1988).
[7] I. Wallace, J. Ryter, and W. H. Breckenridge, J. Chem. Phys. **96**, 136 (1992).
[8] I. Wallace, J. G. Kaup, and W. H. Breckenridge, J. Phys. Chem. **95**, 8060 (1991).
[9] C. Kittel, *Introduction to Solid State Physics*, 6th ed. (Wiley, New York, 1986), p. 58.
[10] S. L. Laursen and H. E. Cartland, J. Chem. Phys. **95**, 4751 (1991).
[11] R. R. Bennett and W. H. Breckenridge, J. Chem. Phys. **92**, 1588 (1990).
[12] R. R. Bennett and W. H. Breckenridge, J. Chem. Phys. **96**, 882 (1992).
[13] H. Umemoto, T. Ohnuma, H. Ikeda, S. Tsunashima, K. Kuwahara, F. Misaizu, and K. Fuke, J. Chem. Phys. **97**, 3282 (1992).
[14] S. Martrenchard-Barra, C. Jouvet, C. Lardeux-Dedonder, and D. Solgadi, J. Chem. Phys. **98**, 5281 (1993).
[15] O. Roncero, J. Beswick, N. Halberstadt, and B. Soep, in *Dynamics of Polyatomic van der Waals Complexes* (Plenum, New York, 1990), Vol. 227; A. Bastida, J. Requena, B. Soep, N. Halberstadt, and J. Beswick, J. Chim. Phys. **92**, 384 (1995).
[16] J. G. McCaffrey and P. N. Kerins, J. Chem. Phys. **106**, 7885 (1997).
[17] J. G. McCaffrey and P. N. Kerins (unpublished).
[18] This was achieved by setting the primary monochromator at a wavelength of 250 nm and monitoring the variation in the intensity of the reflected radiation during deposition. Sample thickness (d) was evaluated using the equation $d=m\lambda/2n\cos\theta$, where m is the number of interference fringes recorded, λ is the wavelength of the incident radiation (250 nm), n the index of refraction of the solid (e.g., $n_{\mathrm{Ar}}=1.30$) and θ is the angle of incidence (22.5°).
[19] D. V. O'Connor and D. Phillips, *Time Correlated Single Photon Counting* (Academic, London, 1984).
[20] G. Zimmerer, Nucl. Instrum. Methods A **308**, 178 (1991).
[21] ZFIT program Nonlinear Least Squares Analysis of Fluorescence Decay Data by M. Rehorek, H. Otto, W. Rettig, and A. Klock, last update August 1995.
[22] V. A. Bracken, Ph.D. thesis, National University of Ireland, Maynooth, 1997.
[23] Steady-state and time-resolved measurements of the pairs of emission bands in the Zn/RG systems exhibit a reversible temperature dependence above 10 K which is discussed in the paper directly following.
[24] The λ^3 extrapolation of the gas phase radiative lifetime of a level m is made on the basis of the expression for the Einstein A coefficient, $A_{mn}=(64\pi^4/3h\lambda^3)\mu^2_{mn}=1/\tau_m$.
[25] R. L. Fulton, J. Chem. Phys. **61**, 4141 (1974).
[26] Tai-ichi Shibuya, J. Chem. Phys. **78**, 5175 (1983).
[27] The indices of refraction of Ar at 219 and 238 nm are 1.324 and 1.317, respectively, at 6 K. Those of Kr at 239 and 258 nm are 1.428 and 1.418, respectively, P. Gürtler (unpublished).
[28] J. R. Fuhr and W. L. Wiese, Atomic Transition Probabilities, 10-179, *CRC Handbook of Chemistry and Physics*, edited by D. R. Lide, 73rd ed. (CRC, Boca Raton, 1993).
[29] A. Fukuda, Phys. Rev. B **1**, 4161 (1970).
[30] D. Le Si Dang, R. Romestain, D. Simkin, and A. Fukuda, Phys. Rev. B **18**, 2989 (1978).
[31] A. Wasiela, Y. Merle d'Aubigne, and R. Romestain, J. Phys. C **13**, 3057 (1980).
[32] A. Fukuda, J. Phys. Soc. Jpn. **40**, 776 (1976).
[33] D. Le Si Dang, R. Romestain, Y. Merle d'Aubigne, and A. Fukuda, Phys. Rev. Lett. **38**, 1539 (1977).
[34] A. Ranfagni, D. Magnai, M. Bacci, G. Viliani, and M. P. Fontana, Adv. Phys. **32**, 823 (1983).
[35] Y. Toyozawa and M. Inoue, J. Phys. Soc. Jpn. **21**, 1663 (1966).
[36] The spin–orbit coupling constant of the $4p$ orbital of atomic zinc is calculated from the general formula $\zeta(np)=2/3|\Delta E|$, where ΔE is $E_{J\max}-E_{J\min}$, the energy difference between the maximum and minimum spin orbit levels. For $J=2$ and $J=0$ at 32 890.317 and 32 311.308 cm^{-1}, respectively, $\zeta(4p)$ of atomic zinc is 386 cm^{-1}. The exchange interaction energy has been estimated from the gas phase energy levels as half the energy difference between the ^1P term and the energetic ''center of gravity'' of the ^3P states at 46 745 and 32 697 cm^{-1}, respectively. This approach is valid only for elements of low atomic mass such as zinc, in which Russell–Saunders coupling occurs.
[37] C. Froese-Fischer, *The Hartree-Fock Method for Atoms-A Numerical Approach* (Wiley, New York, 1977), and references therein.
[38] J. G. Kaup and W. H. Breckenridge, J. Phys. Chem. **99**, 13701 (1995).
[39] The convolution integral $A(t)$ is written as $A(t)=\exp\{-t/\tau\}\int^t_{-t}\exp\{t/\tau\}I(t)\,dt$, where $I(t)$ is the temporal profile of the excitation pulse and τ is the emission decaytime. See J. N. Demas, *Excited State Lifetime Measurements* (Academic, New York, 1983), Chap. 4.